



1 Determining the Plio-Quaternary uplift of the southern French massif-Central; a new insights for in-
2 traplate orogen dynamics.

3 Oswald Malcles¹, Philippe Vernant¹, Jean Chéry¹, Pierre Camps¹, Gaël Cazes^{2,3}, Jean-
4 François Ritz¹, David Fink³.

5 ¹Geosciences Montpellier, CNRS-University of Montpellier, Montpellier, France

6 ²SEES, University of Wollongong, Wollongong, Australia

7 ³Australian Nuclear Science and Technology Organisation, Lucas Heights, Australia

8 *Correspondence to:* Oswald Malcles (oswald.malcles@umontpellier.fr)

9 **Abstract.**

10 The evolution of intra-plate orogens is still poorly understood. Yet, this is of major importance for understand-
11 ing the Earth and plate dynamic, as well as the link between surface and deep geodynamic processes. The
12 French Massif Central is an intraplate orogen with a mean elevation of 1000m, with the highest peak elevations
13 ranging from 1500m to 1885m. However, active deformation of the region is still debated due to scarce evi-
14 dence either from geomorphological or geophysical (i.e. geodesy and seismology) data. Because the Cévennes
15 margin allows the use of karst sediments geochronology and morphometrical analysis, we study the vertical dis-
16 placements of that region: the southern part of the French Massif-Central. Geochronology and morphometrical
17 results, helped with lithospheric-scale numerical modelling, allow, then, a better understanding of this intraplate-
18 orogen evolution and dynamic.

19 Using the ability of the karst to durably record morphological evolution, we first quantify the incision
20 rates. We then investigate tilting of geomorphological benchmarks by means of a high-resolution DEM. We fi-
21 nally use the newly quantified incision rates to constrain numerical models and compare the results with the ge-
22 omorphometric study.

23 We show that absolute burial age (¹⁰Be/²⁶Al on quartz cobbles) and the paleomagnetic analysis of karstic clay
24 deposits for multiple cave system over a large elevation range correlate consistently. This correlation indicates a
25 regional incision rate of $83.4^{+17.3}_{-5.4}$ m.Ma⁻¹ during the last ca 4 Myrs (Plio-Quaternary). Moreover, we point out
26 through the analysis of 55 morphological benchmarks that the studied region has undergone a regional south-
27 ward tilting. This tilting is expected as being due to a differential vertical motion between the north and southern
28 part of the studied area.

29 Numerical models show that erosion-induced isostatic rebound can explain up to two-thirds of the regional up-
30 lift deduced from dating technics and are consistent with the southward tilting obtain from morphological analy-
31 sis. We presume that the remaining part is related to dynamic topography or thermal isostasy due to the Massif
32 Central plio-quaternary magmatism.

33 **1 Introduction and Tectonic Setting**

34 Since the past few decades, plate-boundary dynamics is to a first order, well understood. Such is not the case for
35 intraplate regions, where short-term (10³-10⁵ yrs.) strain rates are low and the underlying dynamical processes



36 are still in debate (e.g. Calais et al., 2010; Vernant et al., 2013; Calais et al., 2016; Tarayoun et al., 2017). On ge-
37 ological time-scales, transient phenomenon that are classically used to explain intraplate deformations (as seen
38 through the seismic activity) can't be a satisfactory explanation though, this then raises the question of the origin
39 of the high finite deformations observed in many parts of the world as for instance the Ural mountains in Russia,
40 the Blue Mountains in Australia or the French Massif Central.

41 In this study we focus on the Cevennes Mountains and the Grands Causses regions that form the southern part
42 of the French Massif Central, located in the southwestern Eurasian plate (fig.1). The region is characterized by a
43 mean elevation of 1000 m with summits higher than 1500 m. Such topography is the result of recent, active up-
44 lift and as the Cevennes mountains experiences an exceptionally high mean annual rainfall (the highest peak,
45 Mount Aigoual, records the highest mean annual rainfall in France of 4015 mm) it raises the question of a possi-
46 ble link between erosion and uplift as previously proposed for the Alps (Champagnac et al., 2007; Vernant et al.,
47 2013; Nocquet et al., 2016). This region currently undergoes a small but discernible deformation, but no signifi-
48 cant quantification can be deduced due to the scarcity in seismicity (Manchuel et al., 2018). In addition, GPS
49 velocities are below the uncertainty threshold of GPS analyses (Nocquet et Calais, 2003; Nguyen et al., 2016).

50 South and West of the crystalline Cevennes mountains, prominent limestone plateaus, named Grands Causses,
51 rise to 1000m and are dissected by several canyons. The initiation of incision, its duration and the geomorphic
52 processes leading to the present-day landscape remain poorly constrained. A better understanding of the pro-
53 cesses responsible for this singular landscape would bring valuable information on intraplate dynamics, espe-
54 cially where large relief exists.

55 The oldest formations in the area were formed during the Variscan orogeny (late Palaeozoic, ~300 Myrs ago;
56 Bricchau et al., 2007) and constitute the crystalline basement of the Cevennes. Between 200 and 40 Myrs ago
57 (Mesozoic and lower Cenozoic), the region was mainly covered by the sea ensuring the development of an im-
58 portant detrital and carbonate sedimentary cover, which can be more than 9 km thick in some locations (Sanchis
59 and Séranne, 2000; Barbarand et al., 2001). During the Mesozoic era, an episode of regional erosion and alter-
60 ation (called the Durancian isthmus) is proposed as being at the origin of the flat, highly elevated surface that
61 persists today across the landscape (Bruxelles, 2001; Husson, 2014).

62 The area is also affected by the major NE-SW trending Cevennes fault system. During the Pyrenean orogeny, 85
63 to 25 Ma (Tricart, 1984; Sibuet et al., 2004), several faults and folds affected the geological formations south of
64 the Cevennes fault, while very few deformations occurred further north within the Cévennes and Grand Causses
65 areas (Arthaud and Laurent, 1995). Eventually, the Oligocene extension (~30 Myrs ago) led to the counterclock-
66 wise rotation of the Corso-Sardinian block and the opening of the Gulf of Lion, re-activating some of the older
67 compressive structures as normal faults. The main drainage divide between the Atlantic Ocean and the Mediter-
68 ranean Sea is located in our study area and is inherited from this extensional episode (Séranne et al., 1995; San-
69 chis et al., 2000).

70 These two tectonic episodes (Pyrenean compression and Oligocene extension) are the main geodynamic pro-
71 cesses that shaped the large-scale structural morphology of the region. Afterwards during the Plio-Quaternary
72 period, only intense volcanic activity has affected the region, from the Massif Central to the Mediterranean
73 shoreline. This activity is characterised by several volcanic events that are well constrained in age (Dautria et
74 al., 2010). The last eruption occurred in the Chaîne des Puys during the Holocene (i.e. the past 10 kyrs (Nehlig



75 et al., 2003; Miallier et al., 2004). Some authors proposed that this activity is related to a hotspot underneath the
76 Massif Central (Granet et al., 1995; Baruol and Granet, 2002) leading to an observed positive heat-flow anomaly
77 and a possible regional plio-Quaternary uplift.

78 Despite this well described overall geological evolution the onset of active incision that has shaped the
79 deep valleys and canyons (e. g. Tarn or Vis river, Fig 1) across the plateaus, and the mechanisms that controlled
80 this incision are still in debate. One hypothesis proposes that canyon formation was driven by the Messinian
81 salinity crisis with a drop of more than 1000m in Mediterranean Sea level. This, however, would then not ex-
82 plain the fact that the Atlantic watersheds show similar incision. Other studies suggested that the incision is con-
83 trolled by the collapse of cave galleries that lead to fast canyon formation mostly during the late Quaternary,
84 thus placing the onset of canyon formation only a few hundreds of thousands of years ago (Corbel, 1954). In
85 contrast, it has also been proposed more recently (based on relative dating techniques and sedimentary evidence)
86 that incision during the Quaternary was negligible (i.e. less than a few tens of meters), and that the regional mor-
87 phological structures seen today occurred around 10 Myrs ago (Séranne et al., 2002; Camus, 2003).

88 In this paper, we provide new quantitative constraints on both the timing of incision and the rate of riv-
89 er down-cutting in the central part of the Cévennes and of the Grands Causses that has resulted in the large relief
90 between plateau and channel bed. We employ two methods, cosmogenic $^{10}\text{Be}/^{26}\text{Al}$ burial dating quartz cobbles
91 that have been transported by rivers and paleomagnetic analyses along vertical profiles of endokarstic clay both
92 of which have been deposited in multiple cave systems at the time cave entry was at river channel elevation. In
93 parallel, by analysing a high-resolution DEM (5m), we show that the region is affected by a regional tilt. Our re-
94 sults allow to quantify the role of the Plio-Quaternary incision on the Cévennes landscape evolution and to con-
95 strain numerical modelling from which we derive the regional uplift rates and a tilt of geomorphological mark-
96 ers.

97 One important point of this study is the integration of multi-disciplinary approaches in order to con-
98 strain intraplate deformation. Such an approach is necessary to bring new insights into the lithosphere behaviour
99 of slow dynamic regions. If the uplift is easily recognisable in the landscape (1000 m high plateaus), quantifying
100 its timing and evolution rates is harder and can't be performed by classical technics (e.g. GPS). This is why we
101 aim to quantify the incision rate over the longest possible period thanks to the karstic immunity. Dealing with
102 long-term incision rates (up to 5 Myrs) should permit to smooth possible climatic-driven incision rate variations
103 (with time-span of several kyrs).

104 If incision is initiated by uplift centred on the North of the area where elevations are maximum, it will lead to
105 tilting of fossilised topographic markers as strath terraces. Our method of analyses provides an opportunity to
106 select between three possible explanations for the current terrain morphology. The first is based on old uplift
107 and old incision (Fig. 2.A). In this case, apparent incision rates would be very low. For instance, if incision com-
108 menced 10 Myrs ago (Serrane et al., 2002), we would find surface tilting but cosmogenic burial dating with
109 $^{10}\text{Be}/^{26}\text{Al}$ which cannot discern ages older than $\sim 5\text{Ma}$ due to excessive decay of ^{26}Al , would not be possible.
110 The second possibility (Fig. 2.B) is that the uplift is old, and incision consequently follows but with a time lag.
111 Here the incision rate would be rather fast but no tilting is expected for the river-related markers because no dif-
112 ferential uplift occurs after their formation. Finally, the third possibility (Fig 2.C) is that uplift and incision are



113 concurrent and recent (i.e. within the time scale of cosmogenic burial dating) and thus we would expect burial
114 ages < 5 Myrs relatively high incision rates, and tilting of morphological markers. These different proposals for
115 the temporal evolution of the region will then be compared using numerical modelling.

116 **2. Determining the incision rates in the Cévennes and the Grand Causses Region**

117 **2.1. Principles and methods**

118 **2.1.1. Karst model**

119 No evidence of important aggradation events has been reported in the literature for the studied area. Therefore
120 we base our analysis on a per descensum infill model of the karst networks whereby sediments are transported
121 and then deposited within cave galleries close to base level. When cave-systems and entry passages are near the
122 contemporaneous river channel elevation (including higher levels during floods), the deposition into caves of
123 sediments, from clay to cobbles occurs, especially during flood events. With subsequent river incision into
124 bedrock creating a relative base level drop (due to uplift or sea-level variations). The galleries associated with
125 the former base-level are now elevated above the new river course and become disconnected from further deposi-
126 tion. Hence fossilised and trapped sediments throughout the cave network represent the cumulative result of
127 incision. In this commonly used model (Granger et al., 1997; Audra et al., 2001; Stock et al., 2005; Harmand et
128 al., 2017), the higher the gallery elevation (relative to the present-day base level) the older the deposits in that
129 gallery. As a result, the objective here is to quantify a relative lowering of the base level in the karst systems,
130 with the sediments closest to the base level being the youngest deposits, and note that we do not date the cave
131 network creation which may very well pre-date river sediment deposition.

132 Within individual canyons, successions of gallery networks across the full elevation range from plateau top to
133 modern river channel, were not always present and often sampling could not be conducted in a single vertical
134 transect. Thus we make the assumption of lateral altitudinal continuity i.e. that within a watershed, which may
135 contain a number of canyons, the sediments found in galleries at the same elevation were deposited at the same
136 time. Inside one gallery, we use the classical principle of stratigraphy sequence (i.e. the older deposits are below
137 the younger ones).

138 **2.1.2. Burial ages**

139 Burial dating using Terrestrial cosmogenic nuclides (TCN) are nowadays a common tool to quantify incision
140 rates in karstic environment (Granger et Muzikar, 2001; Stock et al., 2005; Moccochain., 2007; Tassy et al.,
141 2013; Granger et al., 2015; Calvet et al., 2015; Genti, 2015; Olivetti et al., 2016; Harmand et al., 2017; Rovey II
142 et al., 2017; Rolland et al., 2017; Sartégou, 2017; Sartégou et al., 2018). This method relies on the differential
143 decay of TCN in detrital rocks that were previously exposed to cosmic radiation before being trapped in the
144 cave system. With this in mind, the ^{10}Be and ^{26}Al nuclide pair is classically used as (i) both nuclides are pro-
145 duced in the same mineral (i.e. quartz), (ii) their relative production ratio is relatively well constrained (we use
146 here a standard $^{26}\text{Al}/^{10}\text{Be}$ pre-burial ratio of 6.75, see Balco et al., 2008) and (iii) their respective half-lives



147 (about 1.39 Myr and 0.70 Myr for ^{10}Be and ^{26}Al , respectively) are well suited to karstic and landscape evolution
148 study, with a useful time range of ~ 100 ky to ~ 5 Myr.

149 To quantify the incision rate of the limestone plateau of the Cevennes area, we analysed quartz cobbles infilling
150 from four caves of the Rieutord canyon (Fig. 1), this canyon is well suited for such study because horizontal
151 cave levels are tiers over 200 m above the current river-level and are directly connected to the canyon, leading
152 to a straight relationship between river elevation and the four cave infilling that we have sampled (Cuillère cave,
153 Route cave, Camp-de-Guerre cave and Dugou cave). Furthermore, cobbles source is well known and identified:
154 the upstream part of the Rieutord river, some tens of kilometres northward, providing a uniform sediment origin.
155 All samples (Example Fig. 3) were collected far enough away ($>20\text{m}$) from the cave entrance and deep enough
156 below the surface ($>30\text{m}$) to avoid secondary in-situ cosmogenic production of ^{10}Be and ^{26}Al in the buried sedi-
157 ments.

158 The quartz cobbles were first crushed and purified for their quartz fraction by means of sequential acid attack
159 with Aqua-Regia ($\text{HNO}_3 + 3\text{HCl}$) and diluted Hydrofluoric acid (HF). Samples were then prepared according to
160 ANSTO's protocol (see Child et al. 2000) and $\sim 300\mu\text{g}$ of a ^9Be carrier solution was added to the purified quartz
161 powder before total dissolution. AMS measurements were performed on the 6MV SIRIUS AMS instrument at
162 ANSTO and results were normalised to KN-5-2 (for Be, see Nishiizumi et al., 2007) and KN-4-2 (for Al) stan-
163 dards. Uncertainties for the final ^{10}Be and ^{26}Al concentrations include AMS statistics, 2% (Be) and 3% (Al) stan-
164 dard reproducibility, 1% uncertainty in the Be carrier solution concentration and 4% uncertainty in the natural
165 Al measurement made by ICP-OES, in quadrature. Sample-specific details and results are found in table 1.

166 For the four caves, we observed a good relationship between burial ages and incision, except for the Cam-
167 p-de-Guerre cave (CDG) site, the higher the cave is, the older the burial ages are. Burial ages for the Cuillère
168 cave, Dugou cave, Camp-de-Guerre cave and Route cave are 2.16 ± 0.154 , 0.95 ± 0.137 , 0.63 ± 0.097 and 0.21
169 ± 0.1 Myrs respectively.

170 2.1.3. Paleomagnetic analysis

171 In parallel with burial dating, we collected 141 clay-infilling samples into two main cave systems: the
172 *Grotte-Exurgence du Garrel* and the *Aven de la Leicasse* (Fig. 1). These two sites allowed us collecting sam-
173 ples along a more continuous range of elevations than the one provided by the Rieutord samples and also al-
174 lowed extending the spatial coverage to the Southern Grands Causses region. Thanks to the geometry of these
175 two cave systems, we sampled a 400m downward base level variation. The sampling was done by means of
176 Plexiglas cubes with a 2 cm edge length (Fig. 4) used as a pastry cutter. We weren't able to analyse clay samples
177 from Rieutord canyon because no reliable clay infilling was found in the Rieutord caves.

178 Demagnetisation was performed with an applied alternative field up to 150mT using a 2G-760 cryogenic mag-
179 netometer, equipped with the 2G-600 degausser system controller. Before this analysis, each sample remained at
180 least 48h in a null magnetic field, preventing a possible low coercivity viscosity overprinting the detrital rema-
181 nent magnetisation (DRM) (Hill, 1999; Stock et al., 2005; Hajna et al., 2010). If the hypothesis of instantaneous
182 locked in DRM seems reasonable compared with the studied time span, it is important to keep in mind that the
183 details of DRM processes (as for instance the locked in time) is not well understood (Tauxe et al., 2006; Spassov



184 et Valet, 2012) and could possibly lead to small variations (few percents) in the following computed incision
185 rates.

186 Because fine clay particles are expected being easily reworked in the cave, careful attention was paid to the site
187 selection and current active galleries were avoided. Clays deposits had to show well laminated and horizontal
188 layering in order to prevent analysis of in-situ produced clays (from decalcification) or downward drainage by
189 an underneath diversion gallery that could strongly affect the obtained inclination (and also the declination to a
190 minor extent). Note that for paleo-polarities study alone, small inclination or declination variations won't result
191 in false polarities

192 **2.2 Quantifying the average incision rates**

193 **2.2.1. Rieutord incision rate from burial ages**

194 The relationship between burial ages and incision is shown in Figure 5. Except for the Camp-de-Guerre
195 cave (CDG) site, the higher the cave is, the older the burial ages are. This is consistent with the supposed cave
196 evolution and first-order constant incision of the Rieutord canyon. CDG age has to be considered with caution.
197 The CDG cave entrance located in a usually dry thalweg can act as a sinkhole or an overflowing spring depend-
198 ing on the intensity of the rainfall. The sample was collected in a gallery showing evidence of active flooding
199 ~10 m above the Rieutord riverbed, therefore the older than expected age, given the elevation of the cave, is
200 probably due to cobbles that came from upper galleries during flood events. Forcing the linear regression to go
201 through the origin, leads to an incision rate of $82.8 \pm 34.9 \text{ m.Ma}^{-1}$. These results show that at least half of the
202 300 m deep Rieutord Canyon is a Quaternary incision. Extrapolating the obtained rate yields an age of 4.4 ± 1.9
203 Ma for the beginning of the canyon incision, which suggests that the current landscape has been shaped during
204 the Plio-Quaternary period. To extend our spatial coverage and bring stronger confidence into our results, we
205 combine Rieutord burial ages with paleomagnetic data from watersheds located on the other side of the Hérault
206 watershed.

207 **2.2.2. South Grands Causses incision rate from paleomagnetic data**

208 Of the two cave systems, the lowest sample elevation above sea level (a.s.l.) is in the Garrel (ca 190 m) and the
209 highest in the Leicasse (ca 580 m a.s.l.). Given the very marginal difference in elevation between the local base
210 levels from these two caves, we assume that they have the same local base level reference. In the Leicasse cave
211 system, we sampled 8 sites for a total of 61 samples. Their elevations are located between ca 200 m and ca 400
212 m above base level (a.b.l.), defined as the elevation of the Buèges river spring at 170 m above sea level.

213 From 5 sites, the 80 Garrel samples encompass elevations range between 20 m and 80 m a.b.l. defined by the
214 Garrel spring at 180 m a.s.l.

215 Because one site is a vertical profile of samples and can count between 3 to 15 samples (fig. 4), the figure 6 rep-
216 represents the magnetic polarities by individual sites, in respect with their elevation a.b.l. If all the samples of one
217 site have the same polarity, the site is granted with the same polarity. If not, that is to say if the site displays nor-
218 mal and reverse polarities, we consider it as a transitional site.

219 First, we note a good agreement between samples located at the same elevation, preventing from a possible par-



220 tial endokarstic reworking. Second, the different elevations of the galleries where we collected the samples al-
221 low us to propose that the Leicasse and the Garrel deposits encompass at least three and one polarity chrons, re-
222 spectively. Furthermore, Les Gours sur Pattes (LGP) sampling site record a reversal signal, the lower samples
223 being “reverse”, the upper ones “normal” and the sample in between show a transitional signal (Fig. 7). This
224 specific site provides strong constraints on the age of the sediment emplacement in the magnetostratigraphic
225 timescale (Fig. 6).

226 Although poorly constrained since it relies on a single sample with reverse polarity at (90 m a.b.l.), the eleva-
227 tion/polarity results for the Garrel agrees with U-Th ages younger than 90 kyrs obtained for two speleothems
228 that cover our sampled clays in the Garrel at ca 40 m a.b.l. (Camus, 2003) (Fig. 6). Since no reversed polarities
229 have been found beneath the speleothems despite 72 collected samples, we assume that the emplacement of
230 these clays deposits occurred during the most recent normal period and are therefore younger than 0.78 Ma. The
231 transition between the highest normal sample and the reversed one is located somewhere between 78 m and 93
232 m a.b.l. suggesting a base level lowering rate of $109.6 \pm 9 \text{ m.Ma}^{-1}$.

233 Unfortunately our sampling resolution prevent us from studying possible variations of the incision rate through
234 time. Given our results for the Rieutord samples we assume that the incision rate can be considered to the first
235 order as linear through time. Therefore, we computed theoretical age models for every clay sample, from both
236 the Garrel and the Leicasse cave systems, as a function of various incision rates ranging from 0 to 200 m.Ma^{-1}
237 with a 1 m.Ma^{-1} step. Then, from the magnetostratigraphic timescale, we extracted the theoretical polarity for
238 each sample and computed a correlation factor based on the consistency between the observed polarities and the
239 modelled ones. We obtained 10 possible incision rates with the same best correlation factor (Fig. 8) spanning
240 from 43 to 111 m.Ma^{-1} (mean of $87.2 \pm 23.8 \text{ m.Ma}^{-1}$). Taking into account the transitional signal of the LGP site
241 in the Leicasse cave yields a linear incision rate of $83.4^{+17.3}_{-5.4} \text{ m.Ma}^{-1}$. Proposed uncertainties are based on pre-
242 vious and next transition-related estimated incision rate.

243 Using a similar approach for the Rieutord crystalline samples, we determined a linear incision rate of 85 ± 11
244 m.Ma^{-1} (Fig 8). Those two results, based on independent computations, suggest the same first-order incision rate
245 for the last 4 Ma of $84.2^{+20.5}_{-12.3} \text{ m.Ma}^{-1}$. Given that the Rieutord, Garrel and Buèges rivers are all tributaries of
246 the Hérault river, we propose that this rate represents the incision rate for the Hérault river watershed, inducing
247 approximately 300-350 m of finite incision over the Plio-Quaternary period.

248 If the landscape is at first order in an equilibrium state, that is to say, if we preclude our incision rates being a re-
249 gressive erosional signal, the incision needs to be balanced by an equivalent amount of uplift. If the uplift rate is
250 roughly correlated to the regional topography, lowest uplift rates would be expected in the south of our sampling
251 sites inducing regional tilting of morphological benchmarks. In the next part, we search for such evidences that
252 would suggest differential uplift.

253 2.3 Geomorphometrical evidence

254 According to the Massif-Central centered uplift hypothesis, morphological markers such as strath terraces, flu-
255 vio-karstic surfaces or abandoned meanders should display a southward tilting due to differential uplift between
256 the northern and the southern part of the region, with the expected following signals:

257 - The dipping direction of the tilted markers should be parallel to the main gradient of the topography, i.e. be-



258 tween 150°E and 180°E for our studied region. This expectation is the most important one, regarding uncertain-
259 ties on the uplift rate and lithospheric elastic parameters.

260 - A latitudinal tilting trend, i.e. an increase of the tilt angle along the topography gradient. Indeed, null or small
261 tilts are expected near the shoreline and within the maximum uplift area of the Cevennes/Massif Central, while
262 the maximum tilt is expected at a mid-distance between these two regions, i.e. about 50 km inland from the
263 shoreline.

264 - A positive altitudinal tilting trend (an increase in dip angle with altitude). This trend would be representative
265 of the accumulation of finite tilt. However, it supposes a linear relationship between the altitude and the age of
266 the marker formation. If at first order, this straightforward hypothesis seems reasonable for river-controlled
267 markers (e.g. strath terraces), other surfaces are hardly expected to follow such an easy relationship.

268 To investigate these different signals, we used the morphological markers available for the study area
269 (Fig. 9). We used a 5 m resolution DEM analysis to identify the markers corresponding to surfaces with slope <
270 2°. This cut-off slope angle prevents to identify surface related to local deformation such as for example land-
271 slide or sinkhole. The local river slope is on the order of 0.1° so the 2° cut-off angle is far from precluding to
272 identify tilted markers. We also use a criterion based on an altitudinal range for a surface. This altitudinal span is
273 set individually for each surface based on elevation, slope and curves map analysis, and encompass from few
274 meters to tens of meters depending on the size of the marker. We checked 80% of the identified surfaces in the
275 field in order to avoid misinterpretation. The dip direction and angle of the surface is computed in a two steps
276 approach. First, we compute a plan using extracted points from the DEM inside the delimited surface. Second,
277 based on this plan we remove the DEM points with residuals 3 times larger than the standard error and compute
278 more accurate plan parameters. This outlier suppression removes any inaccurate DEM points and correct for in-
279 accurate surface delimitation (e.g. integration of a part of the edge of a strath terrace).

280 Because no obvious initially horizontal markers are known, we propose to correct the marker current slope by
281 the initial one to quantify the tilt since the marker emplacement. To do so we follow the method used by Cham-
282 pagnac et al. (2008) for the Forealps. We identify the drain related to the marker formation and compute its cur-
283 rent local slope and direction. This method assumes that landscapes are at the equilibrium state and that the river
284 slope remained constant since the marker formation. This assumption seems reasonable given the major river
285 profiles and because most of the markers used are far from the watershed high altitude areas precluding a reces-
286 sive erosional signal. Finally, we removed the local river plan from the DEM extracted surface.

287 Following this methodology, we obtained 61 surfaces. We then applied three quality criteria to ensure the ro-
288 bustness of our results: 1) The minimal surface considered is 2500 m² based on a comparison between the 5m
289 resolution DEM and a RTK GPS survey over 3 strath terraces (Hérault river); 2) Final plans with dip angles
290 larger than 2° are removed; 3) The residuals for each geomorphological marker must be randomly distributed
291 without marker edge signal, or clear secondary structuration. Only 38 markers meet those 3 quality criteria.
292 The results show a mean tilt angle of 0.61 ± 0.41 ° with an azimuth of $N150 \pm 40$ °E (Fig. 10).

293 3 Numerical modelling

294 Both geomorphological and geochronological evidence suggest a Plio-Quaternary uplift of the Cevennes area.



295 The origin of such uplift could be associated with several processes: erosion-induced isostatic rebound, dynamic
296 topography due to mantle convection, thermal isostasy, residual flexural response due to the Gulf of Lion forma-
297 tion, etc. For the Alps and Pyrenees mountains, isostatic adjustment due to erosion and glacial unloading has
298 been recently quantified (Champagnac et al., 2007, Vernant et al., 2013; Genti et al., 2016, Chery et al. 2016).
299 Because the erosion rates measured in the Cevennes are similar to those of the Eastern Pyrenees (Calvet et al.,
300 2015, Sartégou et al., 2018a), we investigate by numerical modelling how an erosion-induced isostatic rebound
301 could impact the southern Massif Central morphology and deformation.

302 We define a representative cross-section parallel to the main topographic gradient (i.e. NNW-SSE) and close to
303 the field investigation areas (Figure 11). We study the lithospheric elastic response to erosion with the 2D finite
304 element model ADELI (Hassani et Chery, 1996; Chéry et al. 2016). The model is composed of a plate account-
305 ing for the elasticity of both crust and uppermost mantle. Although the lithosphere rigidity of the European plate
306 in southern Massif central is not precisely known, vertical gradient temperatures provided by borehole measure-
307 ments are consistent with heat flow values ranging from 60 to 70 mW.m² (Lucazeau et Vasseur, 1989). There-
308 fore, we investigate plate thickness ranging from 10 to 50 km as done by Stewart et Watts (1997) for studying
309 the vertical motion of the alpine forelands. We choose values for Young's and Poisson parameters of respective-
310 ly 10¹¹ Pa and 0.25, both commonly used values for lithospheric modelling (e.g. Kooi et Cloetingh, 1992;
311 Champagnac et al. 2007, Chéry et al., 2001). This leads to long-term rigidity of the lithosphere model ranging
312 from 10²¹ to 10²⁵ N.m. Since the effect of mantle viscosity on elastic rebound is assumed to be negligible at the
313 time scale of our models (1 to 2 Myrs), we neglect the visco-elastic behaviour of the mantle. Therefore, the base
314 of the model is supported by an hydrostatic pressure boundary condition balancing the weight of the lithosphere
315 (Fig. 11). Horizontal displacements on vertical sides are set to zero since geodetic measurements show no sig-
316 nificant displacements (Nocquet et Calais, 2003; Nguyen et al., 2016). The main parameters controlling our
317 model are the erosion (or sedimentation) triggering isostatic rebound and the elastic thickness. The erosion pro-
318 file (Fig. 11) is based on topography, our newly proposed incision rate and other studies (Olivetti et al., 2016 for
319 onshore denudation and Lofi et al., 2003; Leroux et al., 2014 for offshore sedimentation). The flexural rigidity
320 controls the intensity and wavelength of the flexural response and ranges from 10²¹ to 10²⁵ N.m. It can be ex-
321 pressed as a variation in elastic thickness (Te) ranging from 4.4 to 96 km (Fig. 12). We also test a possible Te
322 variation between inland and offshore areas. For the following discussion, we use an elastic thickness of 15km
323 corresponding to a value of D of 3.75 x 10²³ N.m⁻¹. In this case, the inland and offshore parts are largely decou-
324 pled and the large sedimentation rate in the Gulf of Lion does not induce a flexural response on the Cévennes
325 and Grands Causses areas. With a maximum erosion rate of 80 m.Ma⁻¹ (Fig 11), the models display uplift rates
326 of 50 m.Ma⁻¹ over more than 100 km. As previously explained, the finite incision is permitted by an equal
327 amount of uplift considering that the incision is not due to regressive erosion. If all tested models show uplift,
328 the modelled amplitudes are smaller than the expected ones. To obtain the same uplift rate than the incision
329 rates, the applied erosion rate over the model must be increased. However, we assume that the landscape is at
330 equilibrium, so, if the erosion rate is increased, it will be higher than the incision rate leading to the decay of re-
331 lief over the area. No evidence of such evolution is found over the region and, if further studies need to be done
332 to quantify the actual erosion rate, we mostly think that a second process is acting, inducing the rest of the uplift
333 that can't be obtained by the erosion-induced isostatic adjustment. Finally, models predict a seaward tilt of the



334 surface at the regional-scale (Fig. 13), in agreement with the observed tilting of morphological markers.

335 4. Discussion

336 We assume that the sediments collected in the karst were deposited per descensum, i.e. we do not know
337 if the galleries existed a long time before or were formed just before the emplacement of the sediments, but the
338 more elevated the sediments are, the older their deposit is. If there is no evidence of an important aggradation
339 episode leading to more a complex evolution as proposed for the Ardèche canyon (Moccochain et al., 2007;
340 Tassy et al., 2013), we point out that small aggradation or null erosion period could, however, be possible. Some
341 processes could explain such relative stability: e.g. variation in erosion (due to climatic fluctuation) or impact of
342 eustatic variations (in river profile, flexural response, etc.). Such transient variations have been shown for the
343 Alps (Saillard et al., 2014; Rolland et al., 2017) and are proposed as being related to climato-eustatic variations
344 and therefore should last 10 to 100 kyrs at most.

345 Based on our sampling resolution, we cannot evidence such transient periods and we must use an average base
346 level lowering rate in the karst, which we correlate to the incision of the main rivers. The TCN-based incision
347 rate derived from the Rieutord samples ($82.8 \pm 34.9 \text{ m.Ma}^{-1}$) is consistent with the one derived from the Garrel
348 (U-Th ages: 85.83 m.Ma^{-1} according to the sole U/Th exploitable result (Camus, 2003)) and from the Garrel-Le-
349 icasse combination (Paleomagnetic approach: $84.2^{+20.5}_{-12.3} \text{ m.Ma}^{-1}$).

350 This mean incision rate of ca. 85 m.Ma^{-1} lasting at least 4 Ma, highlights the importance of the Plio-Quaternary
351 period into the Cévennes and Grand Causses morphogenesis. Furthermore, the 300 to 400 m of incision pre-
352 cludes a relative base level controlled by a sea-level drop. Indeed, documented sea level variations are less than
353 100 m (Haq, 1988, Miller et al., 2005). Furthermore, the Herault river does not show any significant knickpoints
354 or evidence of unsteadiness in its profile as expected if the incision was due to eustatic variations. Therefore, we
355 propose that the incision rate of $\sim 85 \text{ m.Ma}^{-1}$ is due to a plio-quaternary uplift of the Cévennes and Grands
356 Causses region.

357 Other river-valley processes could lead to a local apparent high incision rate as for instance major land-
358 slide or alluvial fan (Ouimet et al., 2008). This hypothesis of an epigenetic formation of the Rieutord is irrele-
359 vant because of i) none of the possible causes had been found in the Rieutord canyon and ii) the consistency of
360 the TCN-based incision rate and the paleomagnetic-based incision rate for two other cave-systems. Indeed, the
361 use of two independent approaches and three locations is a good argument in favour of the robustness of our
362 proposed mean 85 m.Ma^{-1} incision rate. Yet, using more data, particularly burial dating colocalized with clays
363 samples and adding sampling sites would give a stronger statistical validation. In the Lodève basin (Point 4, fig.
364 1), inverted reliefs allow another independent way to quantify minimal incision rate. K/Ar and paleomagnetic
365 dated basaltic flows spanning from 1 to 2 Myrs old that were deposited at the bottom of the former valley
366 (Dautria et al., 2010) are now located at ca 150 m above the current riverbed leading to an average incision rate
367 of $76.5 \pm 10 \text{ m.Myr}^{-1}$, in agreement with karst-inferred incision rates.

368 Furthermore, preliminary results from canyons on the other side of the Grands Causses (Tarn and Jonte) based
369 on in-situ terrestrial cosmogenic dating suggest similar incision rates (Sartegou et al., 2018b) and confirm a re-
370 gional base level lowering of the Cévennes and Grands Causses region during the Plio-Quaternary. This is con-



371 sistent with the similarities of landscapes and lithologies observed both on the Atlantic and Mediterranean wa-
372 tersheds (e.g. Tarn river).

373 Once the regional pattern of the Plio-Quaternary incision established for the Cévennes-Grands Causses
374 area, the next question is how this river downcutting is related to the regional uplift? First order equilibrium
375 shape and absence of major knick points in the main river profiles preclude the hypothesis of regressive erosion.
376 Hence, the incision rate has to be balanced to the first order by the uplift rate. No obvious evidence of active tec-
377 tonic is reported for the area raising the question of the processes responsible for this regional uplift. Very few
378 denudation rates are reported for our study area (Schaller et al., 2001; Molliex et al., 2016; Olivetti et al., 2017),
379 and converting canyon incision rates into denudation and erosion rates is not straightforward, especially given
380 the large karst developed in the area. Using a first order erosion/sedimentation profile following the main topog-
381 raphy gradient direction we have modelled the erosion-induced isostatic rebound. If this process could create be-
382 tween half and two third of the Plio-Quaternary uplift, a previously existent topography is needed to trigger ero-
383 sion so it cannot explain neither the onset of the canyon-carving nor the full uplift rates. Other, processes have to
384 be explored such as dynamic topography or thermal anomaly beneath the Massif-Central, the magmatism re-
385 sponsible for the important increase in volcanic activity since ~ 6 Myrs (Michon et Merle, 2001; Nehlig et al.,
386 2003) could play a major role, notably in the initiation of Plio-Quaternary uplift.

387 5. Conclusion

388 To the contrary of previous studies that focused on one cave, we have shown that combining karst buri-
389 al ages and paleomagnetic analysis of clay deposits in several caves over a large elevation range can bring good
390 constraints on incision rates. This multi-cave system approach diminishes the intrinsic limits of the two single
391 methods: low sampling density (and analysis cost) for the TCN ages and difficulty to set the position of paleo-
392 magnetic results. Our estimated paleo base level ages are Plio-Quaternary (ca. last 4 Ma) and allow to derive a
393 mean incision rate of $83.4^{+17.3}_{-5.4}$ m.Ma⁻¹ for the Cévennes area.

394 The landscape, and especially the river profiles suggest a first-order equilibrium allowing considering
395 the incision rate as an uplift rate. We propose that related erosional isostatic adjustment is of major importance
396 for the understanding of the southern French Massif-Central landscape evolution and explain a large part of the
397 uplift. However, it is not the only process involved and we hypothesize that it could be especially combined
398 with dynamic topography related to the Massif Central magmatism. Both mechanisms imply an uplift centered
399 on the Massif Central and a radial tilt of the geomorphological surfaces. We have shown using a geomorpholog-
400 ical analysis that at least south of the Cévennes, several surfaces are tilted toward the SSE. This kind of study
401 had been performed before on large structures (Champagnac et al., 2007) or endokarstic markers (Granger et
402 Stock, 2004) but it is the first time that it is performed at such scale with small markers. Numerical modelling
403 yields the same pattern of SSE dipping, allowing more confidence in the geomorphometric results.

404 Our multi-disciplinary approach brings the first absolute dating of the Cévennes landscapes and suggests that the
405 present-day morphology is partly inherited from the plio-quaternary erosion-induced isostatic rebound. A strong
406 uplift impact is assumed to be due to magmatic-related dynamic topography that could explain another part of
407 the uplift as well as the onset of such uplift that has afterward been accelerated by the erosion-induced isostatic
408 rebound. These results enlighten the importance of surface processes into lithospheric-scale dynamic and verti-



409 cal deformations in intra-plate domains.

410 An analysis at the scale of the Massif Central is now needed before nailing down our interpretations,
411 but such study will more likely highlight the importance of erosion processes to explain uplift of intraplate oro-
412 gens, and will show that another process is needed for the Massif Central, which will most likely be dynamic to-
413 pography related to magmatism.

414 References

- 415 Arthaud F. et Laurent P.: Contraintes, déformations et déplacements dans l'avant-pays pyrénéen du Languedoc
416 méditerranéen, *Acta*, 8, 142-157, 1995.
- 417 Audra P., Camus H. et Rochette P.: Le karst des plateaux de la moyenne vallée de l'Ardèche : datation par
418 paléomagnétisme des phases d'évolution plio-quadernaires (aven de la Combe Rajeau). *Bull. Soc. Géol. France*,
419 2001, t. 172. N°1, pp. 121-129, 2001.
- 420 Balco, G., Stone, J.O., Lifton, N.A., Dunai, T.J., 2008. A complete and easily accessible means of calculating
421 surface exposure ages or erosion rates from Be-10 and Al-26 measurements. *Quat. Geochronol.* 3, 174–195.
422 2008.
- 423 Barbarand J., Lucazeau F., Pagel M. Et Séranne M.: Burial and exhumation history of the south-eastern Massif
424 Central (France) constrained by en apatite fission-track thermochronology. *Tectonophysics*, 335, 275-290, 2001.
- 425 Barruol G. et Granet M.: A Tertiary astenospheric flow beneath the southern French Massif Central indicated by
426 upper mantle seismic anisotropy and related to the west Mediterranean extension. *Earth and Planetary Science*
427 *Letters* 202 (2002) 31-47, 2002.
- 428 Brichau S., Respaut J.P. et Monié P.: New age constraints on emplacement of the Cévenol granitoids, South
429 French Massif Central, *Int J Earth Sci* 97:725–738, doi: 10.1007/s00531-007-0187-x, 2007.
- 430 Bruxelles L.: Dépôts et altérites des plateaux du Larzac central : causses de l'Hospitalet et de Campestre (Avey-
431 ron, Gard, Hérault) Evolution morphogénétique, conséquences géologiques et implications pour l'aménagement.
432 Université d'Aix-Marseille I, Université de Provence, UFR Sciences géographiques et de l'aménagement.
433 Thèse, spécialité : Milieux physiques méditerranéens, 2001.
- 434 Calais, E., Freed, A. M., Van Arsdale, R., & Stein, S. (2010). Triggering of New Madrid seismicity by late-
435 Pleistocene erosion. *Nature*, 466(7306), 608–611. <http://doi.org/10.1038/nature09258>
- 436 Calais, E., T. Camelbeeck, S. Stein, M. Liu, and T. J. Craig (2016), A new paradigm for large earthquakes in
437 stable continental plate interiors, *Geophys. Res. Lett.*, 43, doi:10.1002/2016GL070815, 2016.
- 438 Calvet M., Gunnell Y., Braucher R., Hez G., Bourlès D., Guillou V., Delmas M. et ASTER team: Cave levels as
439 proxies for measuring post-orogenic uplift : Evidence from cosmogenic dating of alluvium-filled caves in the
440 French Pyrenees. *Geomorphology* 246 (2015) 617- 633 ; doi : 10.1016/j.geomorph.2015.07.013, 2015.



- 441 Camus H.: Vallée et réseaux karstiques de la bordure carbonatée sud-cévenole. Relation avec la surrection, le
442 volcanisme et les paléoclimats. Thèse de doctorat, Université Bordeaux 3, 692 p, 2003.
- 443 Champagnac J.D., Molnar P., Anderson R.S., Sue C. et Delacou B.: Quaternary erosion-induced isostatic re-
444 bound in the western Alps. *Geology*, March 2007 ; v.35 ; no. 3 ; p. 195-198, doi : 10.1130/G23053A.1, 2007.
- 445 Champagnac J-D. van der Beek P. Diraison G. et Dauphin S.: Flexural isostatic response of the Alps to in-
446 creased Quaternary erosion recorded by foreland basin remnants, SE France. *Terra Nova*, Vol 20, No. 3, 213-
447 220, doi : 10.1111/j.1365-3121.2008.00809.x, 2008.
- 448 Chéry J., Zoback M.D. et Hassani R.: An integrated mechanical model of the San Andreas Fault in central and
449 northern California. *J. Geophys. Res.*, 106(B10) :22051. 52,61, 2001.
- 450 Chéry, J., Genti, M. And Vernant, P. Ice cap melting and low-viscosity crustal root explain the narrow geodetic
451 uplift of the Western Alps. *Geophys. Res. Lett.* 43, 1–8 (2016).
- 452 Child D.P., Elliott G., Mifsud C., Smith A.M and Fink D., Sample processing for earth science studies at
453 ANTARES. *Nuclear Instruments and Methods in Physics Research Section B Beam Interactions with Materials*
454 *and Atoms* 172(1-4):856-860 doi: 10.1016/S0168-583X(00)00198-1, 2000.
- 455 Corbel J.: Les phénomènes karstiques dans les Grands Causses. In : *Revue de géographie de Lyon*, vol. 29, n°4,
456 pp. 287-315, doi : 10.3406/geoca.1954.1990, 1954.
- 457 Dautria J.M., Liotard J.M., Bosch D., Alard O.: 160 Ma of sporadic basaltic activity on the Languedoc volcanic
458 line (Southern France): A peculiar cas of lithosphere-asthenosphere interplay. *Lithos* 120 (2010) 202-222, doi:
459 10.1016/j.lithos.2010.04.009, 2010
- 460 Genti M.: Impact des processus de surface sur la déformation actuelle des Pyrénées et des Alpes. *Géophysique*
461 [physics.geo-ph]. Université de Montpellier, 2015. Français. Thèse, 2016.
- 462 Granet M., Wilson M. et Achauer U.: Imaging a mantle plume beneath the French Massif Central. *Earth and*
463 *Planetary Science Letters* 136 (1995) 281-296, 1995.
- 464 Granger, D. E., Kirchner, J. W., et Finkel, R. C.: Quaternary downcutting rate of the New River, Virginia, mea-
465 sured from differential decay of cosmogenic ²⁶Al and ¹⁰Be in cave-deposited alluvium. *Geology*; February
466 1997 ; v. 25 ; no.2 ; p. 107-110, 1997.
- 467 Granger D.E., Gibbon R.J., Kuman K., Clarke R.J., Bruxelles L. Et Caffee M.W.: New cosmogenic burial ages
468 for Sterkfontein Member 2 Australopithecus and Member 5 Oldowan, *Nature Letter* 2015, doi: 10.1038/nature14268, 2015.
- 470 Granger D.E. et Muzikar P.F.: Dating sediment burial with in situ-produced cosmogenic nuclides: theory, tech-
471 niques, and limitations. *Earth and Planetary Science Letters* 188 (2001) 269-281, 2001.
- 472 Granger D.E. et Stock G.M.: Using cave deposits as geologic tiltmeters : Application to postglacial rebound of
473 the Sierra Nevada, California. *Geophysical Research Letters*, vol. 31, L22501, doi : 10.1029/2004GL021403,
474 2004.
- 475 Zupan Hajna N., Mihevc A., Pruner P., Bosák P. 2010. Palaeomagnetic research on karst sediments in Slovenia.
476 *International Journal of Speleology*, 39(2), 47-60. Bologna (Italy). ISSN 0392-6672, 2010.
- 477 Haq B.U., Herdenbol J. Et Vail P.R.: Mesozoic and cenozoic chronostratigraphy and cycles of sea-level change.
478 *Society Economic Paleontologists Mineralogists Special Publication*, 42, 71-108, Tulsa, Oklahoma. 1988.



- 479 Harmand D., Adamson K., Rixhon G., Jaillet S., Losson B., Devos A., Hez G., Calvet M. et Audra P.: Relation-
480 ships between fluvial evolution and karstification related to climatic, tectonic and eustatic forcing in temperate
481 regions, *Quaternary Science Reviews* (2017) 1-19, doi : 10.1016/j.quascirev.2017.02.016, 2017.
- 482 Hassani R. and Chery J., Anaelasticity explains topography associated with Basin and Range normal faulting.
483 *Geology* 24(12):1095. doi: 10.1130/0091-7613(1996)024<1095:AETAWB>2.3.CO;2. 1996.
- 484 Hill C.A., 1999.. Sedimentology and Paleomagnetism of sediments, Kartchner caverns, Arizona. *Journal of*
485 *Cave and Karst Studies* 61(2) : 79-83, 1999.
- 486 Husson E.: Intéraction géodynamique/karstification et modélisation 3D des massifs carbonatés : Implication sur
487 la distribution prévisionnelle de la karstification. Exemple des paléokarsts crétacés à néogènes du Languedoc
488 montpellierain. *Sciences de la Terre. Université Montpellier 2- Sciences et techniques du Languedoc*, 236 p,
489 2014.
- 490 Kooi H., Cloetingh S. et Burrus J.: Lithospheric Necking and Regional Isostasy at Extensional Basins 1. Subsidence
491 and Gravity Modeling With an Application to the Gulf of Lions Margin (SE France), *Journal of Geophysical*
492 *Research* , vol. 97, no. B12, Pages 17,553- 17,571, november 10, 1992.
- 493 Leroux E., Rabineau M., Aslanian D., Granjeon D., Droz L. et Gorini C.: Stratigraphic simulations of the shelf
494 of the Gulf of Lions: testing subsidence rates and sea-level curves during the Pliocene and Quaternary. *Terra*
495 *Nova*, Vol 26, No. 3, 230-238, doi: 10.1111/ter.12091, 2014.
- 496 Lofi J., Rabineau M., Gorini C., Berne S., Clauzon G., De Clarens P., Dos Reis A.T., Mountain G.S., Ryan
497 W.B.F., Steckler M.S. et Fouchet C.: Plio-Quaternary prograding clinoform wedges of the western Gulf of Lion
498 continental margin (NW Mediterranean) after the Messinian Salinity Crisis., *Marine Geology* July 2003; 198 (3-
499 4) : 289-317, doi: 10.1016/S0025-3227(03)00120-8, 2003.
- 500 Lucazeau F. and Vasseur G.: Heat flow density data from France and surrounding margins, In: V. Cermak, L.
501 Rybach and E.R. Decker (Editors), *Tectonophysics*, 164 (1989) 251-258
- 502 Manchuel K., Traversa P., Baumont D., Cara M., Nayman E. Et Durouchoux C.: The French seismic CATA-
503 *logue* (FCAT-17), *Bull Earthquake Eng* (2018) 16:2227–2251, doi: 10.1007/s10518-017-0236-1, 2018.
- 504 Miallier D., Michon L., Evin J., Pilleyre T., Sanzelle S., et Vernet G.: Volcans de la Chaîne des Puys (Massif
505 Central, France) : point sur la chronologie Vasset-Kilian-Pariou-Chopine. *Comptes Rendus Géoscience*, Elsevier
506
- 507 Michon L. et Merle O.: The evolution of the Massif Central rift: Spatio-temporal distribution of the volcanism.
508 *Bulletin de la Society Geologique de France*, 2001, t. 172, n°2, pp. 201-211, doi: 10.1130/172.2.201, 2001.
- 509 Miller, K.G., Kominz, M.A., Browning, J.V., Wright, J.D., Mountain, G.S., Katz, M.E., Sugarman, P.J., Cramer,
510 B.S., Christie-Blick, N., Pekar, S.F.: The Phanerozoic record of global sea-level change. *Science* 310, 1293–
511 1298, doi : 10.1126/science.1116412, 2005.
- 512 Mocochain L.: Les manifestations géodynamiques –Externes et internes- de la crise de salinité messinienne sur
513 une plate-forme carbonatée peri-méditerranéenne : le karst de la basse ardèche (moyenne vallée du Rhône ;
514 France). Thèse de doctorat, Université Aix- Marseille I – Université de Provence U.F.R des Sciences
515 géographiques et de l'aménagement Centre Européen de Recherches et d'Enseignement en Géosciences de
516 l'Environnement., 196 p, 2007.



- 517 Molliex S., Rabineau M., Leroux E., Boulès D.L., Authemayou C., Aslanian D., Chauvet F., Civet F. et Jouët
518 G.: Multi-approach quantification of denudation rates in the Gulf of Lion source-to-sink system (SE-France).
519 *Earth and Planetary Science Letters* 444 (2016) 101-115, doi : 10.1016/j.epsl.2016.03.043, 2016.
- 520 Nehlig P., Boivin P., de Goër A., Mergoil J., Prouteau G., Sustrac G. Et Thiéblemont D.: Les volcans du Massif
521 central. *Revue BRGM: Géologues, Numéro Spécial: Massif central*, 2003.
- 522 Nguyen H. N., Vernant P., Mazzotti S., Khazaradze G. et Asensio E.: 3-D GPS velocity field and its implica-
523 tions on the present-day post-orogenic deformation of the Western Alps and Pyrenees. *Solid Earth*, 7 ; 1349-
524 1363, 2016, doi : 10.5194/se-7-1349-2016, 2016.
- 525 Nocquet J.-M. et Calais E.: Crustal velocity field of western Europe from permanent GPS array solutions, 1996-
526 2001. *Geophys. J. Int.* (2003) 154, 72-88, doi : 10.1046/j.1365-246X.2003.01935.x, 2003.
- 527 Nocquet J.-M., Sue C., Walpersdorf A., Tran T., Lenôtre N., Vernant P., Cushing M., Jouanne F., Masson F.,
528 Baize S., Chéry J. and Van der Beek P.A., Present-day uplift of the western Alps, *Sci. Rep.* 6, 28404; doi:
529 10.1038/srep28404 (2016).
- 530 Olivetti V., Godard V., Bellier O. et ASTER team : Cenozoic rejuvenation events of Massif Central topography
531 (France) : Insights from cosmogenic denudation rates and river profiles. *Earth and Planetary Science Letters* 444
532 (2016) 179-191, doi : 10.1016/j.epsl.2016.03.049 0012-821X, 2016.
- 533 Ouimet, WB, Whipple, KX, Crosby, BT, Johnson, JP, Schildgen, TF. 2008. Epigenetic gorges in fluvial
534 landscapes. *Earth Surface Processes and Landforms* 33: 1993– 2009. doi: 10.1002/esp.1650 Epigenetic. 2008.
- 535 Rolland Y., Petit C., Saillard M., Braucher R., Boulès D., Darnault R. Cassol D. Et ASTER Team: Inner gorges
536 incision history: A proxy for deglaciation? Insights from Cosmic Ray Exposure dating (¹⁰Be and ³⁶Cl) of river-
537 polished surfaces (Tinée River, SW Alps, France). *Earth and Planetary Science Letters*, Elsevier, 2017, 457,
538 pp.271 - 281, doi : 10.1016/j.epsl.2016.10.007. <hal-01420882>, 2017.
- 539 Rovey II C.W., Balco G., Forir M. Et Kean W.F.: Stratigraphy, paleomagnetism, and cosmogenic-isotope burial
540 ages of fossil-bearing strata within Riverbluff Cave, Greene County, Missouri. *Quaternary Research* (2017), 1-
541 13, doi : 10.1017/qua.2017.14, 2017.
- 542 Saillard M., Petit C., Rolland Y., Braucher R., BOulès D.L., Zerathe S., Revel M. Et Jourdon A.: Late Quater-
543 nary incision rates in the Vésubie catchment area (Southern French Alps) from in situ-produced ³⁶Cl cosmogenic
544 nuclide dating: Tectonic and climatic implications, *J. Geophys. Res. Earth Surf.*, 119, 1121–1135, doi:10.1002/
545 2013JF002985. 2014.
- 546 Sanchis E. et Séranne M.: Structural style and tectonic evolution of a polyphase extensional basin of the Gulf of
547 Lion passive margin : the Tertiary Alès basin, southern France. *Tectonophysics* 322 (2000) 219-242, doi :
548 10.1016/S0040-1951(00)00097-4, 2000.
- 549 Sartégou A.: Évolution morphogénique des Pyrénées orientales: apports des datations de systèmes karstiques
550 étagés par les nucléides cosmogéniques et la RPE. *Géomorphologie*. Thèse de l'Université de Perpignan.
551 Français <NNT : 2017PERP0044>. <tel-01708921> , 2017.
- 552 Sartégou, A., Boulès, D. L., Blard, P.-H., Braucher, R., Tibari, B., Zimmermann, L., et al. (2018a). Deciphering
553 landscape evolution with karstic networks_ A Pyrenean case study. *Quaternary Geochronology*, 43, 12–29.
554 <http://doi.org/10.1016/j.quageo.2017.09.005>
- 555 Sartégou A., Mialon A., Thomas S., Giordani A., Lacour Q., Jacquet A., André D., Calmels L., Boulès D.L.,
556 Bruxelles L., Braucher R., Leanni L. Et ASTER team.: When TCN meet high school students: deciphering west-



557 ern Cévennes landscape evolution (Lozère, France) sin g TCN on karstic networks. Poster 4th Nordic Workshop
558 on Cosmogenic Nuclides. 2018b.

559 Schaller M., von Blanckenburg F., Hovius N. Et Kubik P.W.: Large-scale erosion rates from in situ-produced
560 cosmogenic nuclides in European river sediments. *Earth and Planetary Science Letters* 188 (2001) 441-458,
561 2001.

562 Séranne M., Benedicto A., Labaum P., Truffert C. et Pascal G.: Structural style and evolution of the Gulf of
563 Lion Oligo-Miocene rifting : role of the Pyrenean orogeny. *Marine and Petroleum Geology*, Vol. 12, No. 8, pp.
564 809-820, 1995.

565 Séranne M., Camus H., Lucazeau F., Barbarand J. et Quinif Y.: Surrection et érosion polyphasées de la Bordure
566 cévenole. Un exemple de morphogenèse lente. *Bull. Soc. Géol. France*, 2002, t. 173, n°2, pp. 97-112, 2002.

567 Sibuet J.-C., Srivastava S.P. et Spakman W.: Pyrenean orogeny and plate kinematics. *Journal of Geophysical*
568 *Research: Solid Earth*, Vol 109, doi: 10.1029/2003JB002514 , 2004.

569 Spassov S. et Valet J.-P.: Detrial magnetisations from redeposition experiments of different natural sediments.
570 *Earth and Planetary Science Letters* 351-352 (2012) 147-157, dog: 10.1016/j.epsl.2012.07.016, 2012

571 Stewart J. and Watts A.B.: Gravity anomalies and spatial variation of flexural rigidity at mountain ranges. *Jour-*
572 *nal of Geophysical research*, vol 102, no. B3, Pages 5327-5352, march 10, 1997, doi: 10.1029/96JB03664,
573 1997.

574 Stock G.M., Granger D.E., Sasowsky I.D., Anderson R.S. et Finkel R.C.: Coomparison of U-Th, paleomag-
575 netism, and cosmogenic burial methods for dating caves : Implications for landscape evolution studies. *Earth en*
576 *Planetary Science Letters* 236 (2005) 388-403, doi : 10.1016/j.epsl.2005.04.024, 2005.

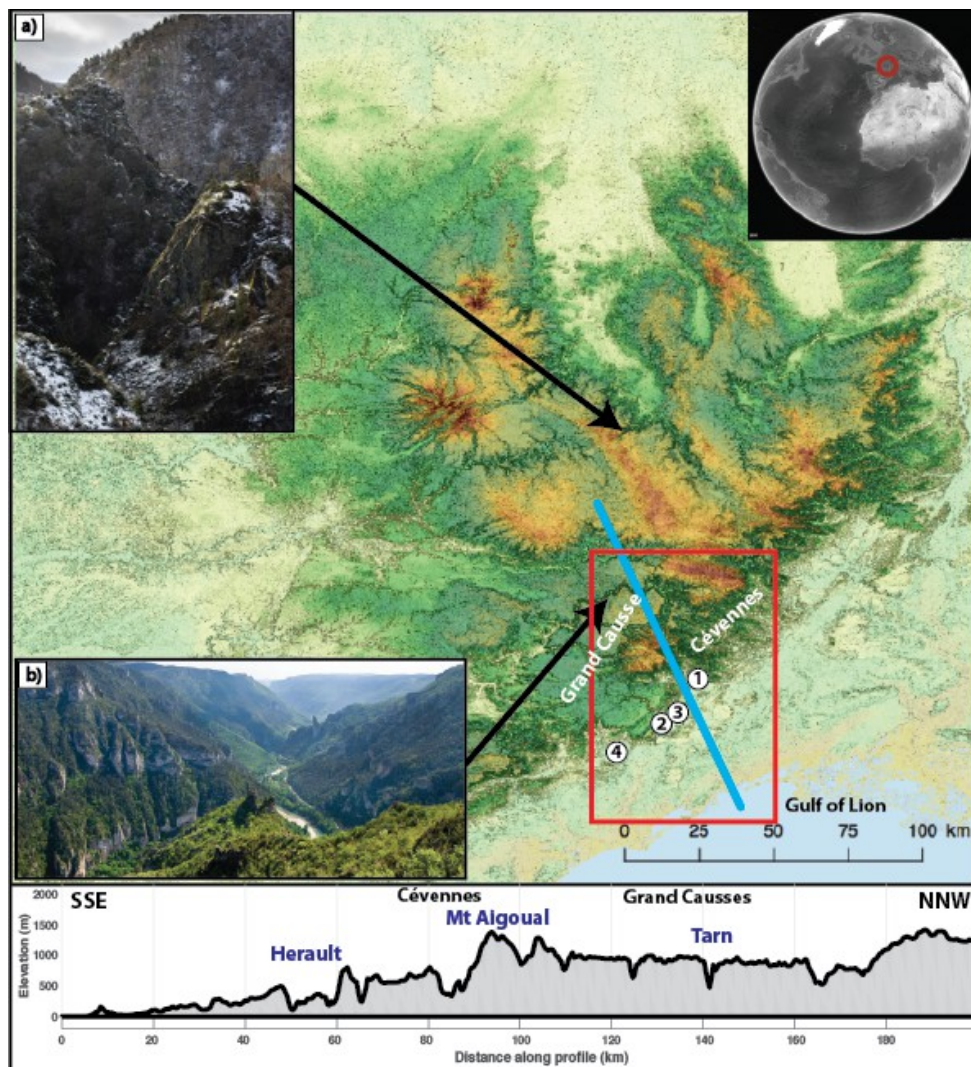
577 Tarayoun A., Mazzotti S., Gueydan F., Quantitative impact of structural inheritance on present-day deformation
578 and seismicity concentration in intraplate deformation zones, *Earth and Planetary Science Letters*, Volume 518,
579 2019, Pages 160-171, ISSN 0012-821X, doi: 10.1016/j.epsl.2019.04.043., 2017.

580 Tassy A., Mocochain L., Bellier O., Braucher R., Gattacceca J., Bourlès D.: Coupling cosmogenic dating and
581 magnetostratigraphy to constrain the chronological evolution of peri-Mediterranean karsts during the Messinian
582 an the Pliocene: Example of Ardèche Valley, Southern France. *Geomorphology*, 189 (2013), pp. 81-92, doi:
583 10.1016/j.geomorph.2013.01.019, 2013.

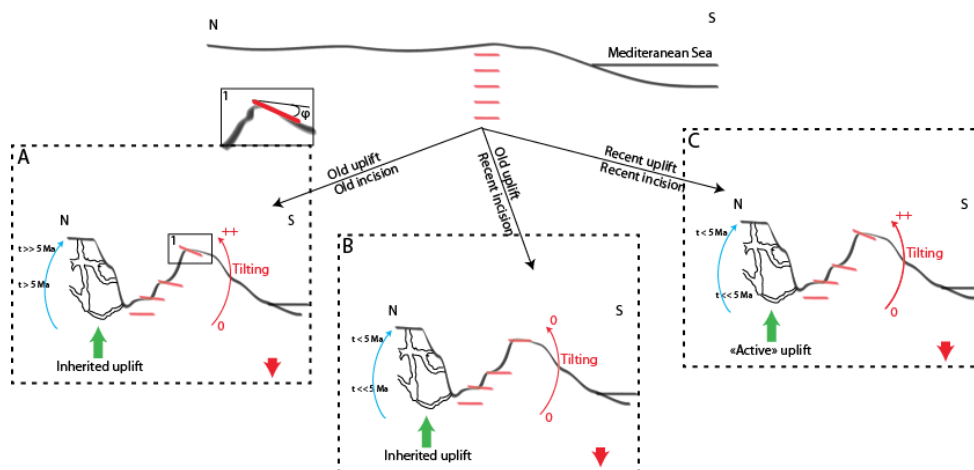
584 Tauxe L., Steindorf J.L. et Harris A.: Depositional remanent magnetisation: Toward an improved theoretical and
585 experimental foundation. *Earth and Planetary Science Letters* 244 (2006) 515-529, doi:
586 10.1016/J.epsl.2006.02.003, 2006.

587 Tricart P. : From passive margin to continental collision: A tectonic scenario for the western Alps. *American*
588 *journal of science*, Vol. 284, February, 1984, P97-120, 1984.

589 Vernant, P., Hivert, F., Chéry, J., Steer, P., Cattin, R., & Rigo, A. (2013). Erosion-induced isostatic rebound
590 triggers extension in low convergent mountain ranges. *Geology*, 41(4), 467–470.
591 <http://doi.org/10.1130/G333942.1>



592 Figure 1: 30 m resolution DEM of the French Massif-Central and slope shadowed. Examples of finite
593 incision typical of the French Massif-Central in a) cristalline area (Seuge Canyon) and b) limestone
594 plateau (Tarn Canyon) Location of the restricted studied area in red box (fig. 8) and numerated site 1) is
595 the Rieutord Canyon, 2) is the Leicasse Cave System and 3) is the Garrel Cave system and 4) is the
596 Lodève bassin with dated basaltic flows. Bottom panel is an example of typical topographic profile used
597 for numerical model set up.



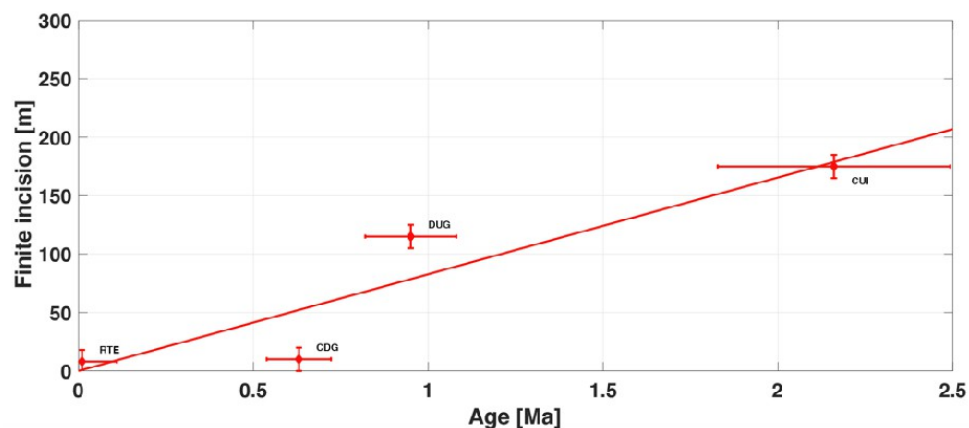
598 **Figure 2:** conceptual models for landscape evolution. Top panel is the initial stage (prior to uplift). Each
599 panel represent a possible scenario explaining current morphology: A) Old uplift and old incision, B) Old
600 uplift and recent incision and C) both recent uplift and incision. Blue arrow and associated ages show ex-
601 pected result (or absence of) for burial dating. Red level represents morphological markers that are
602 fossilised when reaching the surface, accumulating afterward (or not) the differential uplift by finite tilt-
603 ing.



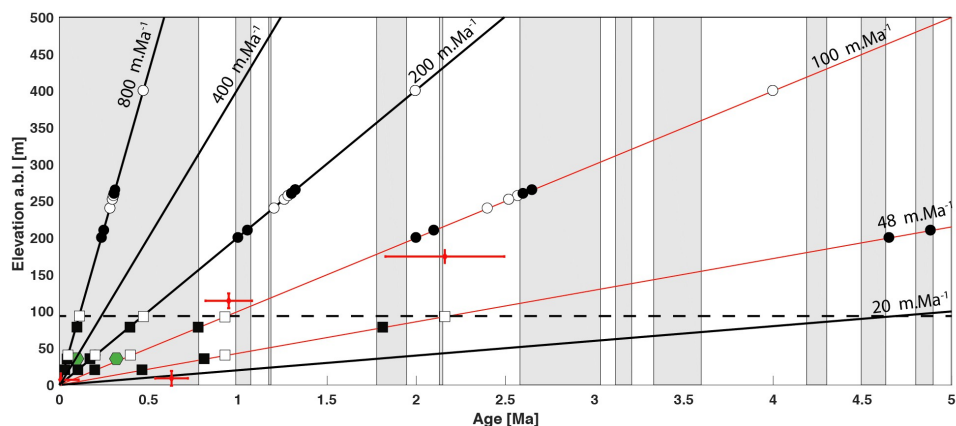
604 **Figure 3:** Example of quartz cobbles sampled for burial dating. Location: Cuillère Cave



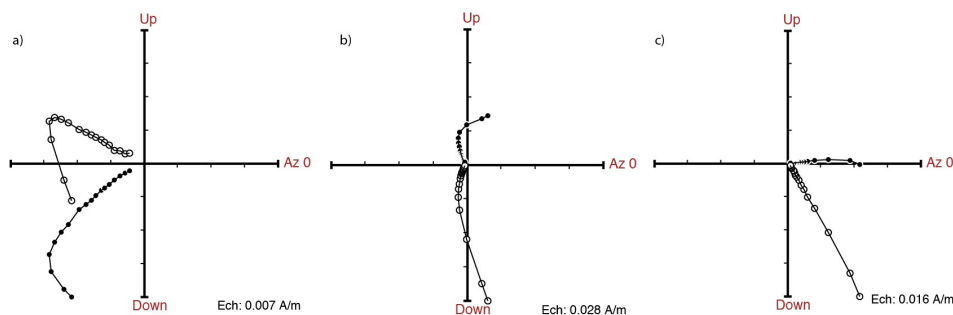
605 **Figure 4: Example of clay sampling for the paleomagnetic study. Location at the entrance shaft (Highest**
606 **elevation of every samples (~580 m a.s.l.), Leicasse Cave system)**



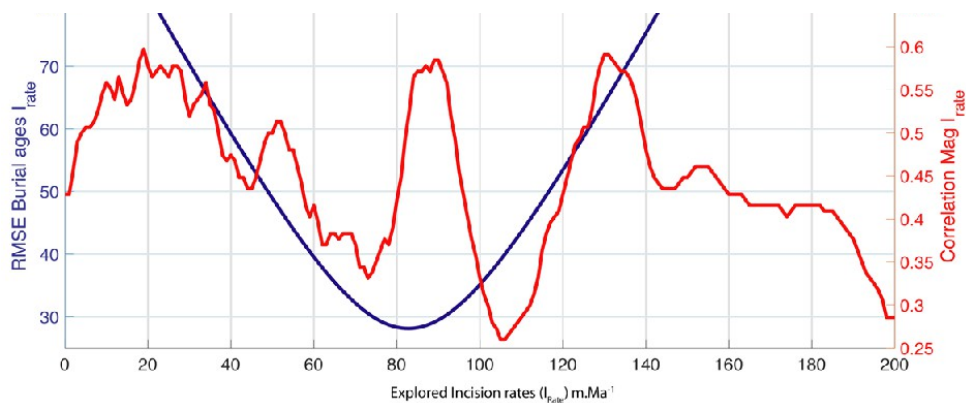
607 **Figure 5: Relation finite incision-burial age for the Rieutord canyon. Finite incision is the elevation of the**
608 **sampling site relatively to the current riverbed. RTE for Route Cave, CDG for Camp de Guerre Cave,**
609 **DUG for Dugou Cave and CUI for Cuillère Cave**



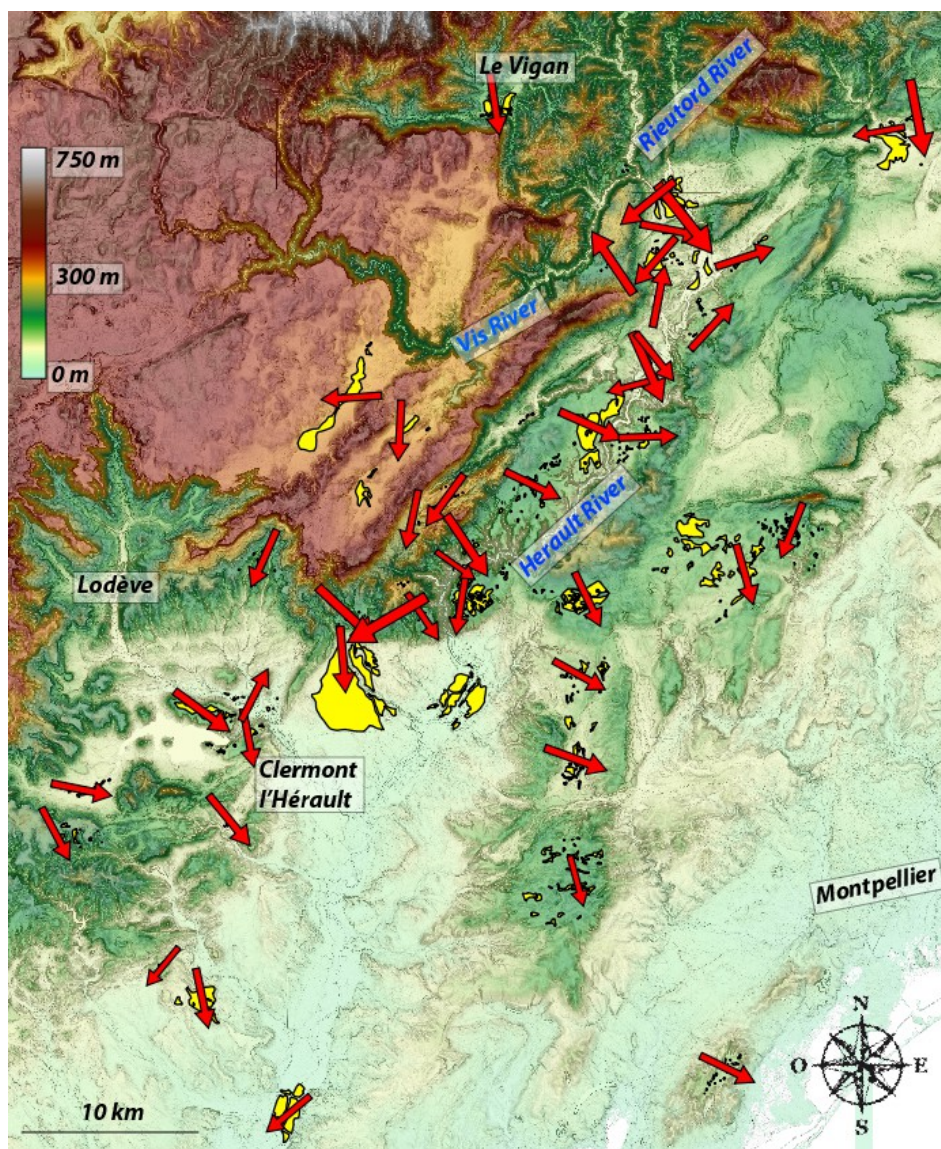
610 **Figure 6: Constraint on the incision rate from plural data set. Circles (Leicasse Cave system) and squares**
 611 **(Garrel Cave system) are paleomagnetic polarities from clay deposits. Black is for Normal polarity, white**
 612 **for Reversed polarity and grey for transitional signal.**
 613 **Each point is representative of one sampling profile including an average of 10 samples per site. Lines**
 614 **represent different linear incision rates with example of good correlation (red ones) and bad correlation**
 615 **(black ones). The horizontal dashed line shows the predicted polarities-age for one site located ~100m**
 616 **a.b.l. This measured reversed polarity match with theoretical red lines but fails with the three other**
 617 **exposed incision-rate.**
 618 **Green hexagons are representation of U/Th ages obtain in the Garrel (Camus, 2003). Burial ages from fig.**
 619 **4 are shown for comparison (Red points)**



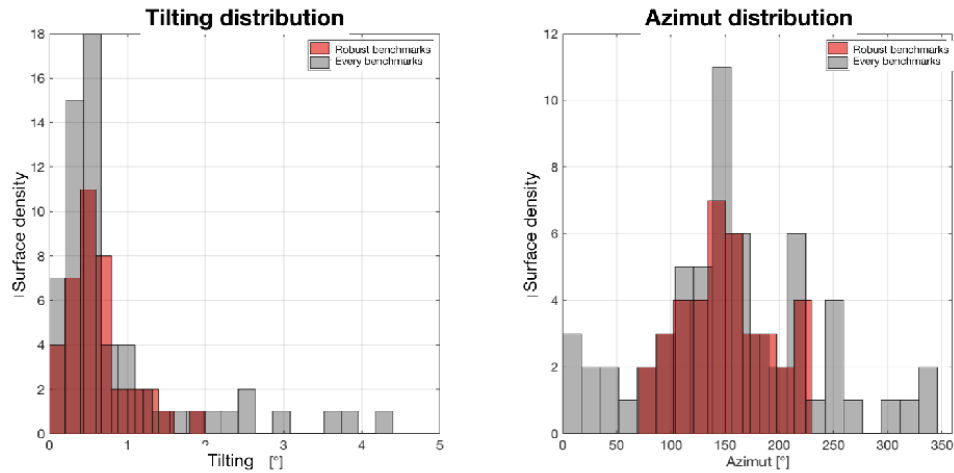
620 **Figure 7: Zijderveld Diagram for three samples from the Gours-sur-Pattes (Leicasse) site. Stratigraphical**
 621 **order is from a) (the older, base of the profile) to c) (the younger, top of the profile).**



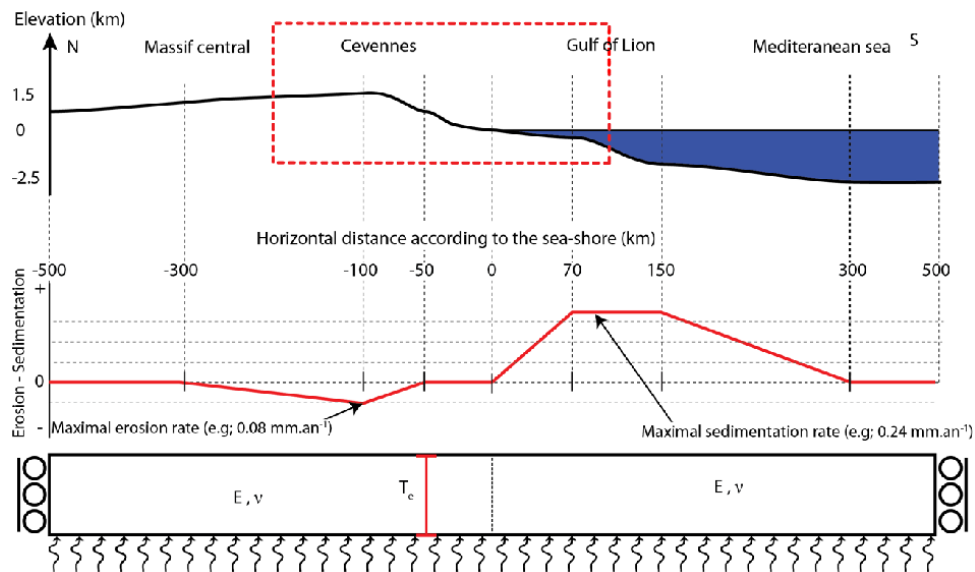
622 **Figure 8: Best incision rate based on paleomagnetic data (Red) and burial ages (blue). The Red curve is**
623 **the normalised correlation between theoretical and observed polarities. The highest correlation**
624 **corresponds to the best incision rates. The blue curve is the RMSE for the linear regression through the**
625 **burial ages data set shown on Fig. 4.**



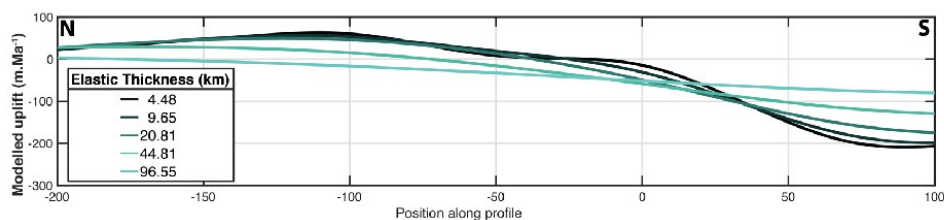
626 Figure 9: Tilting map of geomorphological benchmark (yellow areas). Fond-map is 5 m resolution DEM
627 with slope shadow. Red arrows are orientating according to the marker downward dip and sized
628 according to the corrected tilting angle (the bigger, the more the tilting)



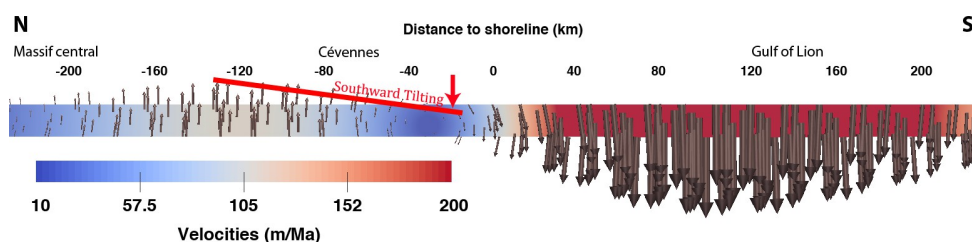
629 **Figure 10: Tilting and azimuth distribution.** Left panel is density distribution for surface maximum
 630 tilting in degree. Right panel is azimuth of maximum dipping relative to the north. For each histogram,
 631 red and grey populations are for robust and primary detected markers.



632 **Figure 11: Top panel: schematic topographic profile.** The studied area that includes the studied zones is
 633 delimited by the red box (cf fig. 1). Middle panel, surface processes profile, negative values are for erosion
 634 and positive values for sedimentation. Bottom panel: model set-up with two compartments (one for the
 635 Cevennes area and the second one for the gulf of lion). The base of the model is compensated in pressure
 636 and the right and left limits are fixed at zero horizontal velocities and free vertical ones. T_e is the
 637 equivalent elastic thickness (in km), E (Pa) and ν are the Young modulus and the Poisson coefficient
 638 respectively whom values are independent in each compartment.



639 **Figure 12: Modelled uplift according to different T_e . Most probable T_e are between 10 and 30 km.**



640 **Figure 13: Modelling result for $T_e=15$ km. Erosion-sedimentation rate profile is the same as in fig. 6.**
 641 **Velocity field is shown using arrow for scale and orientation and colour code for value. Black values on**
 642 **top are distance relative to the sea-shore (positive value landward and negative values seaward). Red line**
 643 **represent the southward modelled tilting due to differential uplift.**

Cave	Lat	Lon	Elevation	height (a.b.l.)	^{10}Be conc (atom/g)	σ ^{10}Be (atom/g)	^{26}Al conc (atom/g)	σ ^{26}Al (atom/g)	$^{26}\text{Al}/^{10}\text{Be}$ (and error)	Burial age (Ma)	Burial age error (Ma)
RTE	43,960	3,707	175	8	3,54E+04	1,18E+03	2,16E+05	1,47E+04	6,11 +/-0.46	0,20	+0.16/-0.15
CDG	43,955	3,710	185	10	8,87E+04	3,12E+03	4,29E+05	3,28E+04	4,83 +/-0.41	0,67	+0.18/-0.16
DUG	43,957	3,711	245	115	1,27E+04	5,68E+02	5,29E+04	6,36E+03	4,15 +/-0.53	0,99	+0.28/-0.25
CUI	43,959	3,711	354	175	1,70E+04	7,14E+02	3,75E+04	5,28E+03	2,20 +/-0.32	2,28	+0.33/-0.28

644 Table 1: Samples analytical results and parameters. Cave code are: RTE for the “de la route” Cave, CDG for the
 645 “Camp de Guerre” cave, DUG for the “Dugou” Cave and CUI for the “Cuillère” Cave. Main parameters are the
 646 geographical coordinate (Lat, Lon in decimals degree), the elevation (a.s.l), the height (a.b.l., computed
 647 relatively to the surface river elevation. The concentration (atoms/g quartz) of ^{10}Be and ^{26}Al in collected sand
 648 samples are all AMS $^{10}\text{Be}/\text{Be}$ and $^{26}\text{Al}/\text{Al}$ isotopic ratios corrected for full procedural chemistry blanks and
 649 normalised to KN-5-4 and KN -4-2, respectively. The error () is for total analytical error in final average ^{10}Be
 650 and ^{26}Al concentrations based on statistical counting errors in final $^{10}\text{Be}/\text{Be}$ ($^{26}\text{Al}/\text{Al}$) ratios measured by
 651 AMS in quadrature with a 1% error in ^9Be spike concentration (or a 4% error in ^{27}Al assay in quartz) and a



652 2% (or 3%) reproducibility error based on repeat of AMS standards. Burial age (minimum) assuming no post-
653 burial production by muons at given depth (all deeper than 30m) in cave below surface and assuming initial
654 $^{26}\text{Al}/^{10}\text{Be}$ ratio is given by the production ratio of 6.75. The burial age error determined by using a $\pm 1\sigma$
655 range in the measured $^{26}\text{Al}/^{10}\text{Be}$ ratio